Preliminary Report on the 16 October 1999 M 7.1 Hector Mine, California, Earthquake

Scientists from the U.S. Geological Survey, Southern California Earthquake Center, and California Division of Mines and Geology

INTRODUCTION

The M_w 7.1 Hector Mine, California, earthquake occurred at 9:46 GMT on 16 October 1999. The event caused minimal damage because it was located in a remote, sparsely populated part of the Mojave Desert, approximately 47 miles east-southeast of Barstow, with epicentral coordinates 34.59°N 116.27°W and a hypocentral depth of 5 ± 3 km. Twelve foreshocks, M 1.9–3.8, preceded the mainshock during the previous twelve hours. All of these events were located close to the hypocenter of the mainshock.

The Hector Mine earthquake occurred within the Eastern California Shear Zone (ECSZ). By virtue of its remote location, the societal impact of the Hector Mine earthquake was, fortunately, minimal in spite of the event's appreciable size. The ECSZ is characterized by high seismicity, a high tectonic strain rate, and a broad, distributed zone of north-northwest-trending faults (ECSZ; Figure 1; Dokka and Travis, 1990; Sauber *et al.*, 1986; Sauber *et al.*, 1994; Sieh *et al.*, 1993). Data regarding the slip rates of faults within the ECSZ suggest that on the order of 15% of the Pacific-North American plate motion occurs along this zone (Sauber *et al.*, 1986; Wesnousky, 1986). Most of the faults in the ECSZ have low slip rates and long repeat times for major earthquakes, on the order of several thousands to tens of thousands of years. The occurrence of the Hector Mine earthquake within seven years and only about 30 km east of the 1992 M_w 7.3 Landers earthquake suggests that the closely spaced surface faults in the ECSZ are mechanically related.

The Hector Mine event involved rupture on two previously mapped fault zones—the Bullion Fault and an unnamed, more northerly-trending fault that is informally referred to in this paper as the Lavic Lake Fault (Dibblee, 1966, 1967a,b). Traces of the Bullion Fault exhibit evidence of Holocene displacement and were zoned as active in 1988 under California's Alquist-Priolo Earthquake Fault Zoning Act (Hart and Bryant, 1997). The pattern of rupture along more than one named fault was also observed from the 1992 Landers earthquake (Hauksson *et al.*, 1993; Sieh *et al.*, 1994).

Much of the fault zone that produced the Hector Mine earthquake had been buried by relatively young stream deposits, and the fault scarps in bedrock have a subdued morphology. It appears that these faults have not experienced significant offset for perhaps 10,000 years or more (Hart, 1987). Planned future investigations will refine the age of the last event on these faults. The portion of the Lavic Lake Fault that ruptured between the northern end of the Bullion Mountains and Lavic Lake had not previously been mapped. However, our field investigations have identified ancient, subdued fault scarps along portions of the 1999 rupture zone in this area. It thus appears that the entire segment of the Lavic Lake Fault that was involved in the 1999 event had ruptured in the past. As is typical for most faults within the Eastern California Shear Zone, the rate of movement along the Lavic Lake Fault may be quite slow (<1 mm/yr) and should produce earthquakes only infrequently. This event is a reminder that faults that have ruptured in late Quaternary time, but that lack evidence of Holocene displacement, can still produce earthquakes in this low-slip-rate tectonic setting.

Additionally, the Hector Mine earthquake is noteworthy for a couple of other reasons. First, it clearly produced triggered seismicity over much of southern California, from the rupture zone toward the south-southwest in particular. Second, as we will discuss, the event may provide new data and insight into recently developed paradigms concerning earthquake interactions and the role of static stress changes.

Questions such as these will, of course, be the subject of extensive detailed analyses in years to come. Fortunately, the Hector Mine sequence will provide one of the best data sets obtained to date for a significant earthquake in the United States. Because it occurred when major upgrades to both the regional seismic network (TriNet) and the regional geodetic network (SCIGN) were well underway, the Earth science community will have abundant high-quality data with which to explore the important and interesting questions that have been raised. In this paper, we present and discuss the basic data and preliminary results from the Hector Mine earthquake.

GEOLOGIC FIELD OBSERVATIONS

On Saturday, 16 November 1999, from 3:00 to 6:00 P.M. (local time), scientists made a helicopter reconnaissance

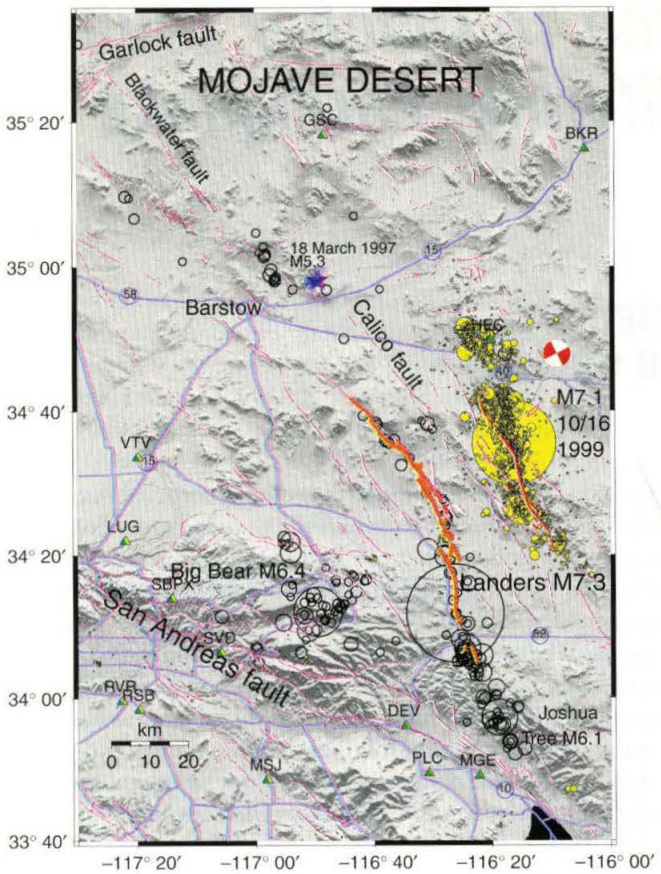

▲ **Figure 1.** Eastern Mojave region including regional faults (light pink lines) and topography (gray-scale). Open black circles indicate seismicity (mainshocks and early aftershocks) associated with the 1992 Joshua Tree-Landers-Big Bear sequence. Filled yellow circles indicate aftershocks of the 10/16/99 Hector Mine earthquake. Red lines show surface rupture associated with the *M* 7.3 Landers earthquake and with the *M* 7.1 Hector Mine earthquake.

▲ **Figure 2.** Simplified map of surface fault rupture associated with the Hector Mine earthquake (yellow). The rupture involved the southernmost portion of the Bullion Fault, previously recognized as Holocene-active, and the previously unnamed "Lavic Lake" fault. Prior to the earthquake, the Lavic Lake Fault had been mapped in the Bullion Mountains only and did not display evidence of Holocene activity. Holocene-active traces of other nearby faults in the vicinity are identified by the dashed white lines. Natural color digital orthoimagery, at .5 meter resolution, was provided by Earth-Data International under contract to the U.S. Marine Corps Air Ground Combat Center, Geospatial Information and Services/Remote Sensing Lab.

flight and found the northwest and southeastern ends of the surface rupture, as well as the area of maximum slip. They made a preliminary map of the fault breaks, upon which flight lines were planned for aerial photography. Military operations resumed all day long on Sunday, 17 October. A set of 275 air photos was then taken at 1:10,000 scale at dawn (for low sun angle) on Monday, 18 October. On 18 and 22–24 October, geological field crews were able to make comprehensive measurements all along the fault zone during a respite in the military training operations at the base.

In the week following the Hector Mine earthquake, up to thirteen teams of geologists from the U.S. Geological Survey, Southern California Earthquake Center, and California Division of Mines and Geology collaborated to map the extent and complexity of surface fault rupture. Faulting with observed right-lateral displacement was traced for approximately 41 km along the mapped traces of the Lavic Lake and Bullion Faults (Figure 2). Minor fault displacements were also observed on splays extending from the main rupture zone and along subparallel fault traces located within a few kilometers of the main zone. Including these additional faults, the overall length of surface faulting is approximately 45 km.

The fault rupture is characterized by linear scarps, right-laterally offset stream channels, mole tracks, trenches, shutter ridges, and left-stepping en echelon fractures commonly connected by thrust faults. Complexity of surface faulting varies from a simple linear scarp to multiple branches within a zone several hundred meters wide. Overall, there was less distributed faulting than was observed from the 1992 Landers earthquake, but there are several regions where fault patterns are quite complex. In particular, distributed rupture occurs between the northern end of the Bullion Mountains and Lavic Lake. Also, a zone of surface rupture about 700 meters wide delineates the complex junction between the Lavic Lake and Bullion Faults. Several kilometers north of the southern end of the rupture, the Bullion Fault bifurcates

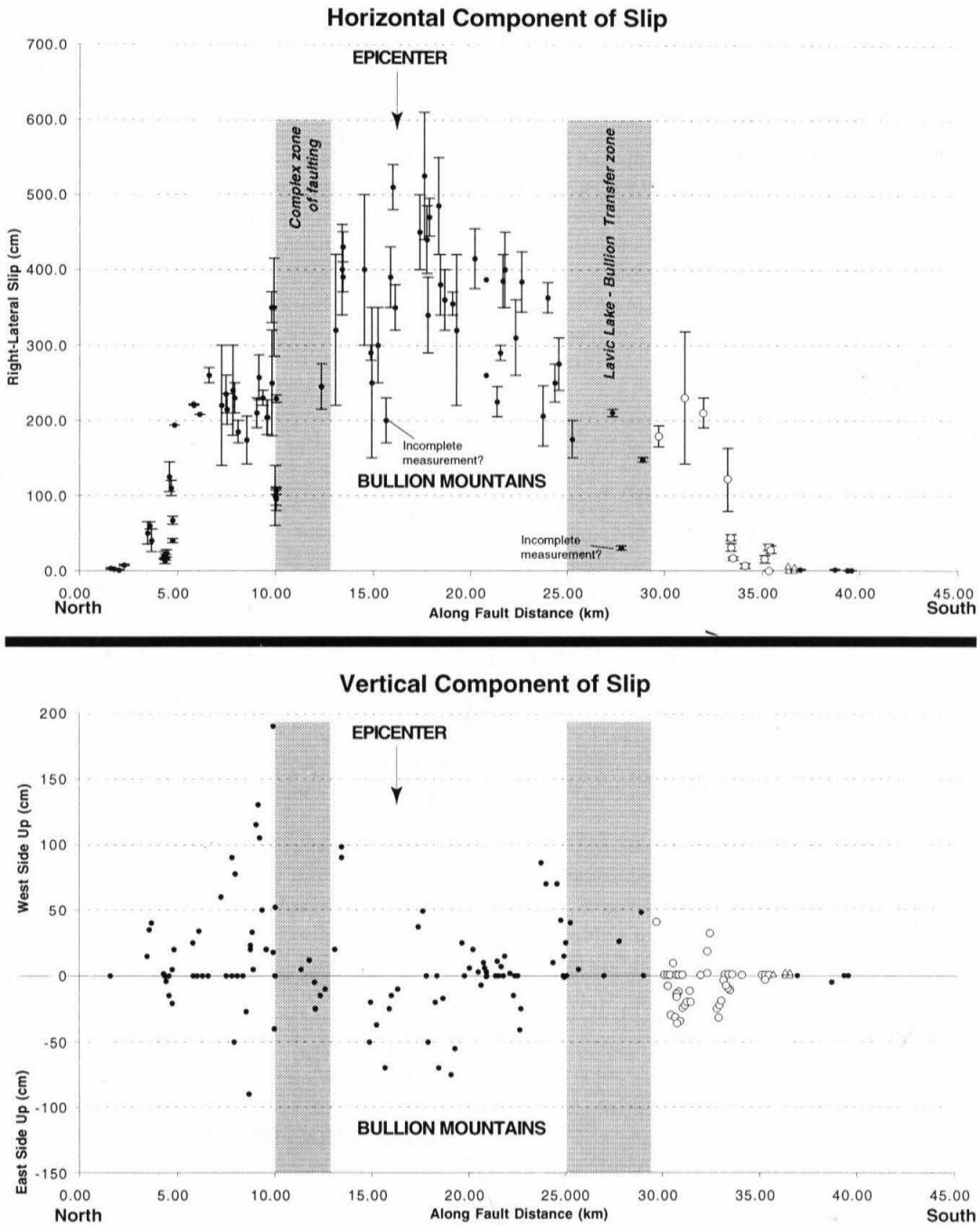

▲ **Figure 3.** Preliminary slip distribution for the Hector Mine earthquake fault rupture taken from field measurements. Open circles represent data from the Wood Canyon area, where rupture occurs on two major parallel strands (slip represents a sum of the average values across the two strands). The open triangles represent data from a parallel western strand southwest of the main rupture zones at the south end of the system. Error bars reflect the total range of uncertainty in the slip estimate as reported by individual investigators.

into two distinct branches about 1 km apart. Both of these previously mapped traces ruptured in this event (Figure 2). The fault rupture map is preliminary and will be refined as more complete observations of fault slip are made.

Slip was measured at over 300 sites along the main rupture. These measurements are combined to form a slip distribution profile along the rupture (Figure 3). Where multiple fault strands are present, total slip values at each site are obtained by summing displacement vectors. Although present data are incomplete, the distribution of horizontal slip along the fault appears to be remarkably symmetrical, with rather abrupt terminations of slip at the ends of the rupture. Although rupture and surface cracking has been observed over a length of more than 40 km, significant horizontal slip (*i.e.*, more than a few centimeters) occurs over a length of less than 35 km. The largest horizontal displace-

ment measured within the first week, 525 ± 85 cm of right-lateral slip, is located approximately 4 km south of the epicenter in the Bullion Mountains.

Preliminary results indicate an average slip across the entire fault zone of approximately 250–300 cm. The largest observed vertical displacement was nearly 200 cm, but values of 100 cm or less were more commonly observed. Overall the sense of this displacement component is not consistent, which is typical for strike-slip ruptures. Between the Bullion Mountains and Lavic Lake, there is consistent west-side-up displacement where the fault curves northward, producing a small releasing bend. East-side-up displacement is observed just to the south of the epicenter where the fault bends westward (a compressive bend).

TriNet: MODERN REAL-TIME SEISMOLOGY

The U.S. Geological Survey, Caltech, and the California Division of Mines and Geology have been running and continuing to develop TriNet, a state-of-the-art broadband and strong-motion seismic network in southern California. TriNet is a multipurpose network designed to record and analyze on-scale ground motions, distribute that information quickly, improve our understanding of earthquakes and their effects, contribute to improving building codes and structural design, and facilitate emergency response in cooperation with other agencies. As of October 1999 there were 120 USGS-Caltech real-time stations online and nearly 200 CDMG strong-motion stations for which data is accessed via a dial-up protocol. Eventually, TriNet will include over 600 stations (see Mori *et al.*, 1997; Hauksson *et al.*, 1999).

The Hector Mine earthquake provided a good mid-project test and evaluation of the performance of TriNet. TriNet is designed so that within the first minute following the recorded shaking from an event, the event epicenter, magnitude, and ground motion parameters are available from the USGS-Caltech component of the network. Within minutes, data from most of the important near-source CDMG stations are reported. A more complete CDMG contribution is available within approximately thirty minutes.

An initial magnitude and location is obtained within minutes of an event using the real-time stations. For the Hector Mine earthquake, a location and preliminary M_L estimate of 6.6 were obtained approximately 90 seconds after the origin time of the event. A magnitude of 7.0 was derived from estimated radiated energy (Kanamori *et al.*, 1993) approximately 30 seconds later.

Location and magnitude estimates for significant events are broadcast via email, the World Wide Web, and pager messages via the CUBE system (Mori *et al.*, 1997). The first CUBE page following Hector Mine, including the M_L 6.6 value, was received approximately 3.5 minutes after the event; an updated page with the estimate M 7.0 was received approximately thirty seconds later.

One critical product of TriNet is "ShakeMap", which involves rapid (within 3–5 minutes) generation of maps displaying ground-motion parameters throughout southern California. These parameters include observed ground motion values as well as intensity values derived from newly developed relationships between recorded ground-motion parameters and expected shaking intensity (Wald *et al.*, 1999a). Estimation of shaking over the entire regional extent of southern California is obtained via spatial interpolation of the measured ground motions, which are recorded on a fairly sparse, nonuniformly spaced network of stations. A uniform sampling grid is obtained using geologically based frequency and amplitude-dependent site corrections (Wald *et al.*, 1999b). The observations are augmented with predicted ground motions in areas without seismic stations, which for this earthquake includes the entire near-fault region.

Production of maps is automatic, triggered by any significant earthquake in southern California (see Wald *et al.*, 1999b for more details). TriNet has provided funds to include ShakeMap as input data for loss-estimation tools used by the California Office of Emergency Services (OES). Although ShakeMap data files were used for rapid loss-estimation calculations for the Hector Mine earthquake, the results were not of significant societal impact because the event occurred in an uninhabited region and caused only moderate shaking in sparsely populated parts of the Mojave Desert.

The first ShakeMap for the Hector Mine earthquake was produced within four minutes of the event. Initially, ShakeMap ground motions in the near-source region were estimated using ground-motion regression from a point source at the epicenter. The map was revised later, as information about fault dimensions became available (Figure 4). Fault dimension information was initially derived from the aftershock distribution and, later, the observed surface trace. Results from both lines of evidence were noted to be consistent with a preliminary finite-fault model determined within hours of the event using waveform data from the TriNet array (D. Dreger, http://www.seismo.berkeley.edu/seismo/eqw/99.10.16_ff.html).

SOURCE MODELING RESULTS

The mainshock hypocenter is located approximately 2 km east of the north end of the Bullion Fault. The first motion focal mechanism is poorly constrained because the SCSN station distribution is sparse in the epicentral region. Mainshock moment tensor solution and centroid depth determinations were performed using data from 60 broadband TriNet stations, ranging from 70 to 400 km in epicentral distances. We use the CAP source inversion technique which utilizes both the P_{nl} and surface wave portions of broadband waveforms to constrain source orientation and depth (Zhu and Helmberger, 1996). The standard southern California velocity model (Hadley and Kanamori, 1979) is used to calculate the Green's functions. The CAP technique allows time shifts between data and synthetics while computing the waveform misfits so that the influences of source mislocation

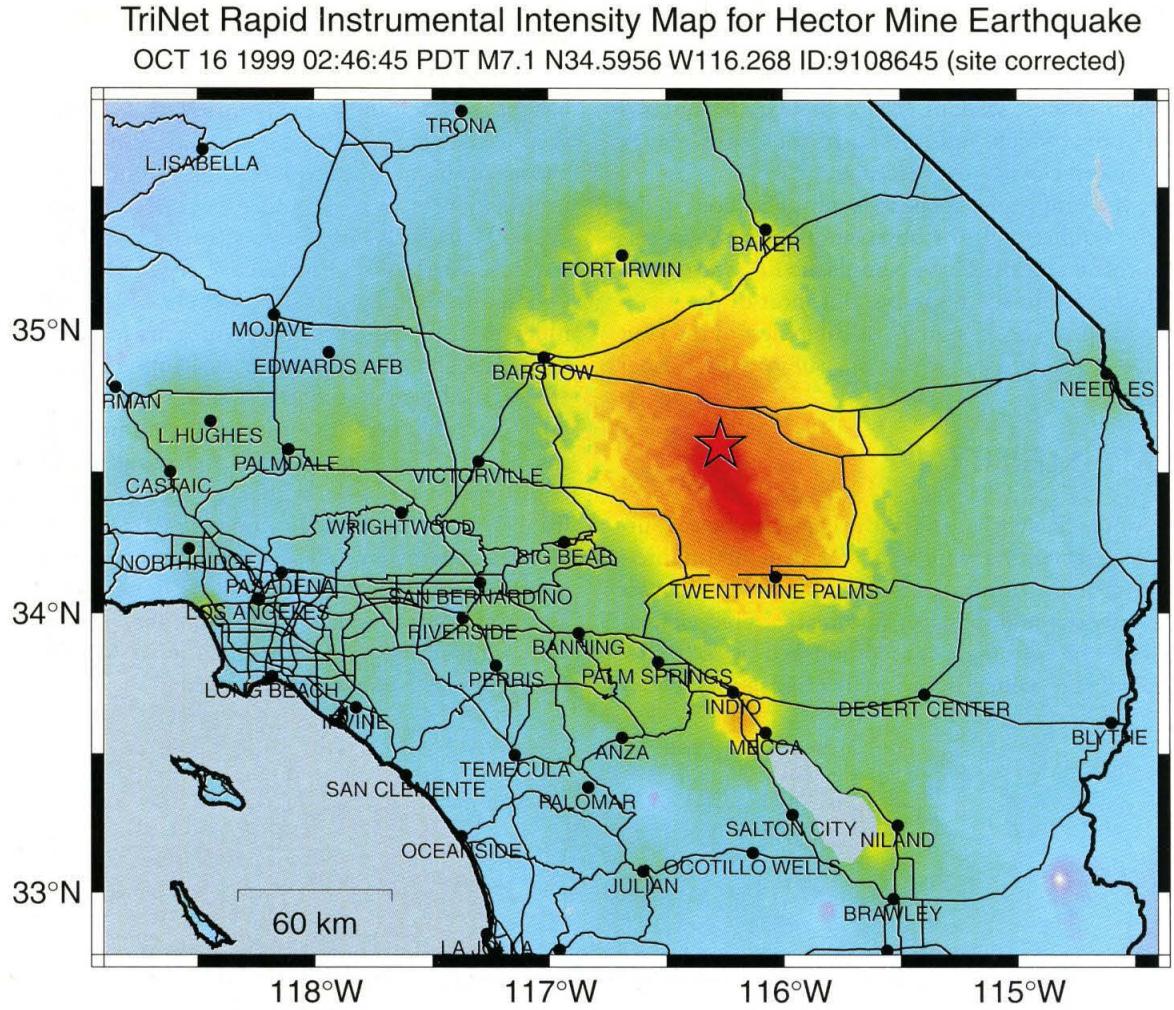

PERCEIVED SHAKING	Not Felt	Weak	Light	Moderate	Strong	Very Strong	Severe	Violent	Extreme
POTENTIAL DAMAGE	None	None	None	Very Light	Light	Moderate	Moderate/Heavy	Heavy	Very Heavy
PEAK ACC.(%g)	*<.17*	*.17-1.4*	*1.4-3.9*	*3.9-9.2*	*9.2-18*	18-34	34-65	65-124	>124
PEAK VEL.(cm/s)	<0.1	0.1-1.1	1.1-3.4	3.4-8.1	8.1-16	*16-31*	*31-60*	*60-116*	*>116*
INSTRUMENTAL INTENSITY	I	II-III	IV	V	VI	VII	VIII	IX	X+

▲ **Figure 4.** TriNet rapid instrumental intensity ShakeMap of the 10/16/99 Hector Mine, California, earthquake. Shaking scale is indicated at bottom of figure.

and crustal heterogeneities are minimized. For this preliminary source inversion, a double-couple point source of 9 s duration is assumed. Figure 5 shows the waveform misfit errors for different source depths where the misfit error is measured by the L2-norm of the difference between the velocity records and synthetics, normalized by the data variance. The optimal centroid depth is determined to be 13.5 km. (Misfit within 10% of the optimal value is obtained for a depth range of roughly 12–15 km).

The optimal fault plane solution has a strike of N29°W and a dip of 77° to the east, with pure right-lateral motion and moment of 3.4×10^{26} Nm (M_w 7.0). The scalar moment is slightly smaller than the estimate derived from

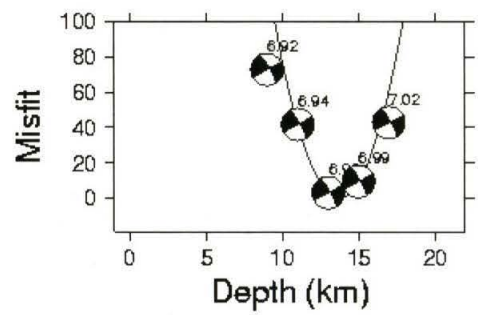

▲ **Figure 5.** Misfit as a function of centroid depth. For each depth, the mechanism and M_w value are also plotted.

teleseismic observations (5.0×10^{26} Nm; S. Sipkin, pers. comm.). Examples of waveform fits for stations surrounding the mainshock at similar distances are presented in Figure 6. The time shifts at these stations do not show significant azimuthal variation, which indicates that the main energy release was located close to the epicenter.

Despite the simple point-source assumption used in the inversion, the synthetics fit the observations well. Some stations such as NEE and BC3 have complicated P_{nl} waveforms which might be due to site response. But most of the waveform misfits are probably caused by the finiteness of the fault and the rupture directivity, which are subjects of further investigations.

COMMUNITY INTENSITY MAP

In addition to the ShakeMap effort, the U.S. Geological Survey is also experimenting with a new system of Internet-based postearthquake information gathering, which focuses on shaking intensity and damage. Automatic, rapid generation of seismic intensity maps is accomplished by collecting shaking and damage reports from Internet users immediately following felt earthquakes in California (see Wald *et al.*, 1999c for more details).

Intensity survey questionnaires, contributed from members of the community using forms made available through the Internet, are converted to numerical intensities based on an algorithm modified from Dengler and Dewey (1998). All information is received and processed through the USGS World Wide Web site; the associated postal ZIP code region is color-coded and an interactive regional intensity map is updated as each report is received. This approach allows for much more rapid generation of intensity maps than the standard, labor-intensive practice of mailing intensity surveys and manually processing the results.

The public response to the Community Internet Intensity Maps ("Did You Feel It?") following the Hector Mine event was enthusiastic, with over 25,000 responses sent in from 1,116 different ZIP codes (Figure 7). Nearly 5,000 responses were received and processed within the first six hours, 10,000 within the first twelve hours. We are still evaluating the robustness of these voluntary responses and we will compare them to more traditional Modified Mercalli Intensities after they are determined.

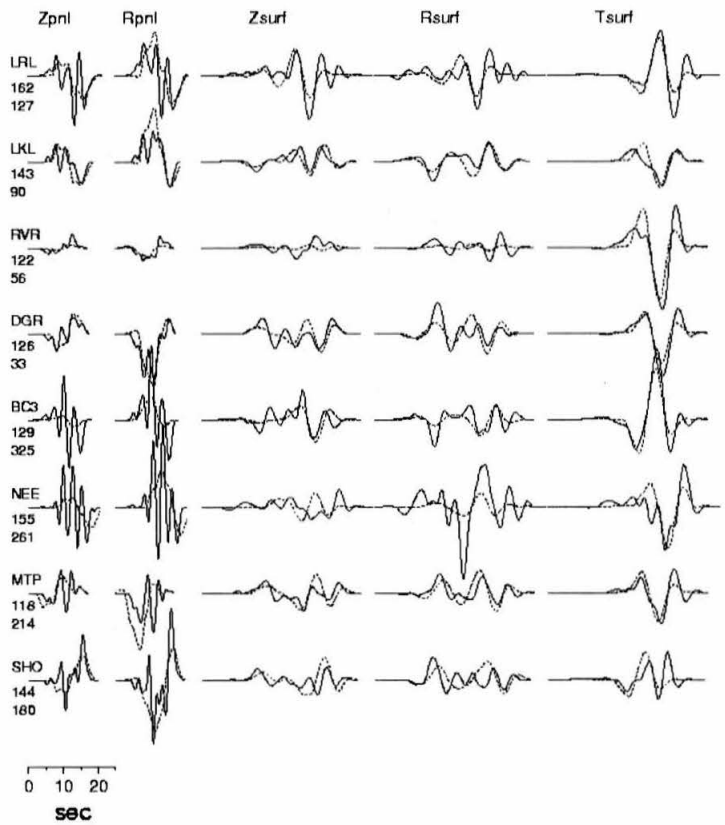

▲ **Figure 6.** Examples of waveform fits for stations surrounding the mainshock at similar distances. Numbers below station names are the epicentral distance in kilometers and the azimuth in degrees. Dark solid lines are velocity records and dashed lines are synthetics corresponding to the optimal moment tensor solution. True amplitudes are preserved except that a distance scaling factor of 1 and a weight of 4 are applied to the P_{nl} waves, and a distance scaling factor of 0.5 and a weight of 1 are used for the surface waves (for details, see Zhu and Helmberger, 1996). The tangential component of the surface wave portion is scaled down by a factor of 2 with respect to the vertical and radial components for presentation.

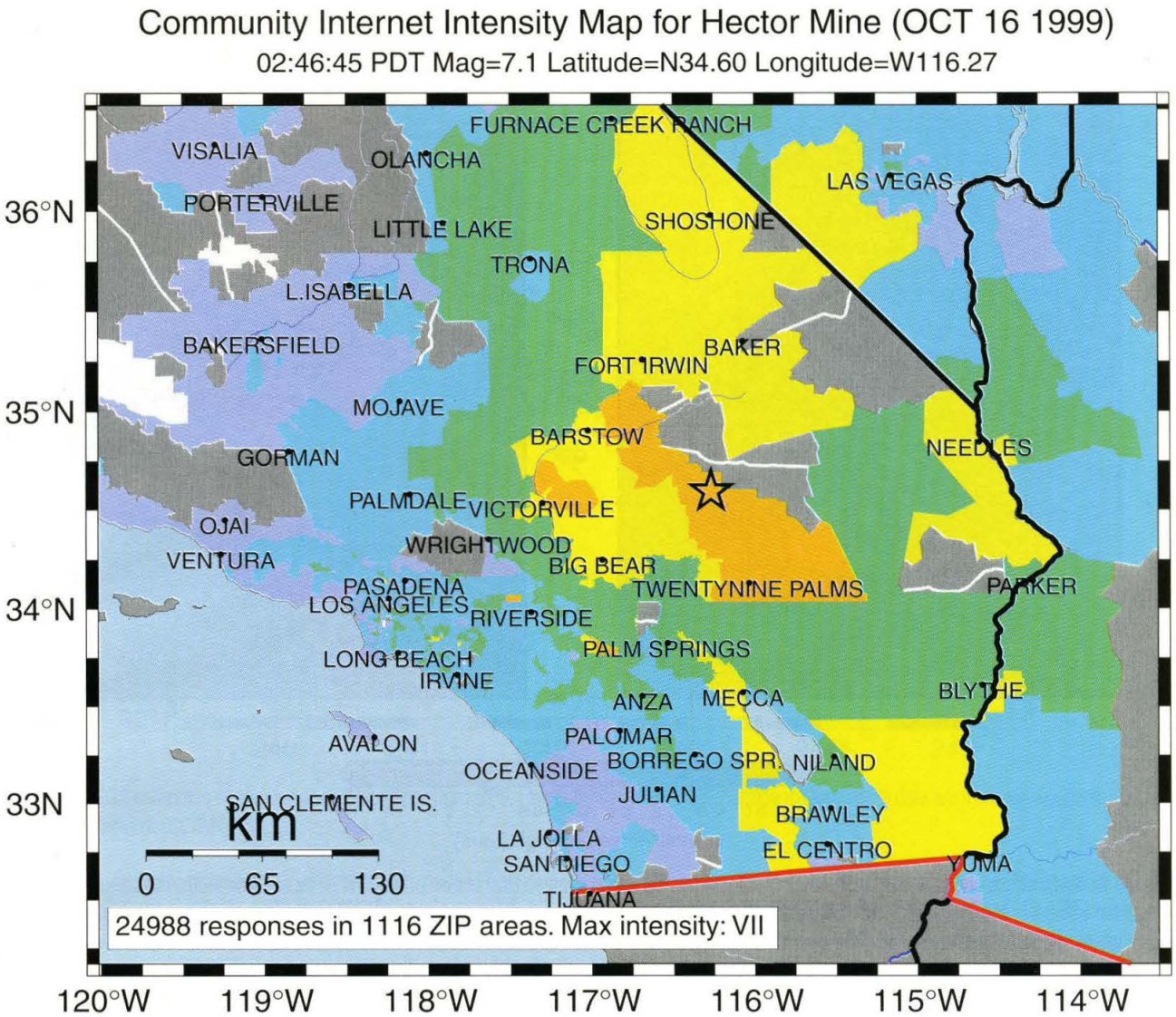

INTENSITY	I	II-III	IV	V	VI	VII	VIII	IX	X+
SHAKING	Not Felt	Weak	Light	Moderate	Strong	Very Strong	Severe	Violent	Extreme
DAMAGE	None	None	None	Very Light	Light	Moderate	Moderate/Heavy	Heavy	Very Heavy

▲ **Figure 7.** Preliminary community Internet intensity map of the Hector Mine mainshock. This map summarizes intensities derived from nearly 25,000 reports from 1,116 different postal ZIP codes.

Both ShakeMap and the Community Internet Intensity Map can be found on the World Wide Web at URL http://www-socal.wr.usgs.gov, from the links "Shake Map" and "Did You Feel It?" Online versions of more detailed manuscripts explaining these systems can be found at those sites.

STRESS-TRIGGERING RESULTS

The Hector Mine earthquake occurred near the location of the 1992 M 7.3 Landers earthquake, suggesting that it may have been triggered by the Landers event. The triggering mechanism, however, is unclear.

Recent earthquake triggering research has primarily focused on static stress transfer. The static stress change on a fault is usually represented by the Coulomb stress change, $\Delta(CS) = \Delta t + m'\Delta s$, where Δt is the change in shear stress in the direction of slip, Δs is the change in normal stress (tension positive), and m' is the apparent coefficient of friction, meant to incorporate the effects of fluid pressure changes. A triggered earthquake occurs in response to a positive Coulomb

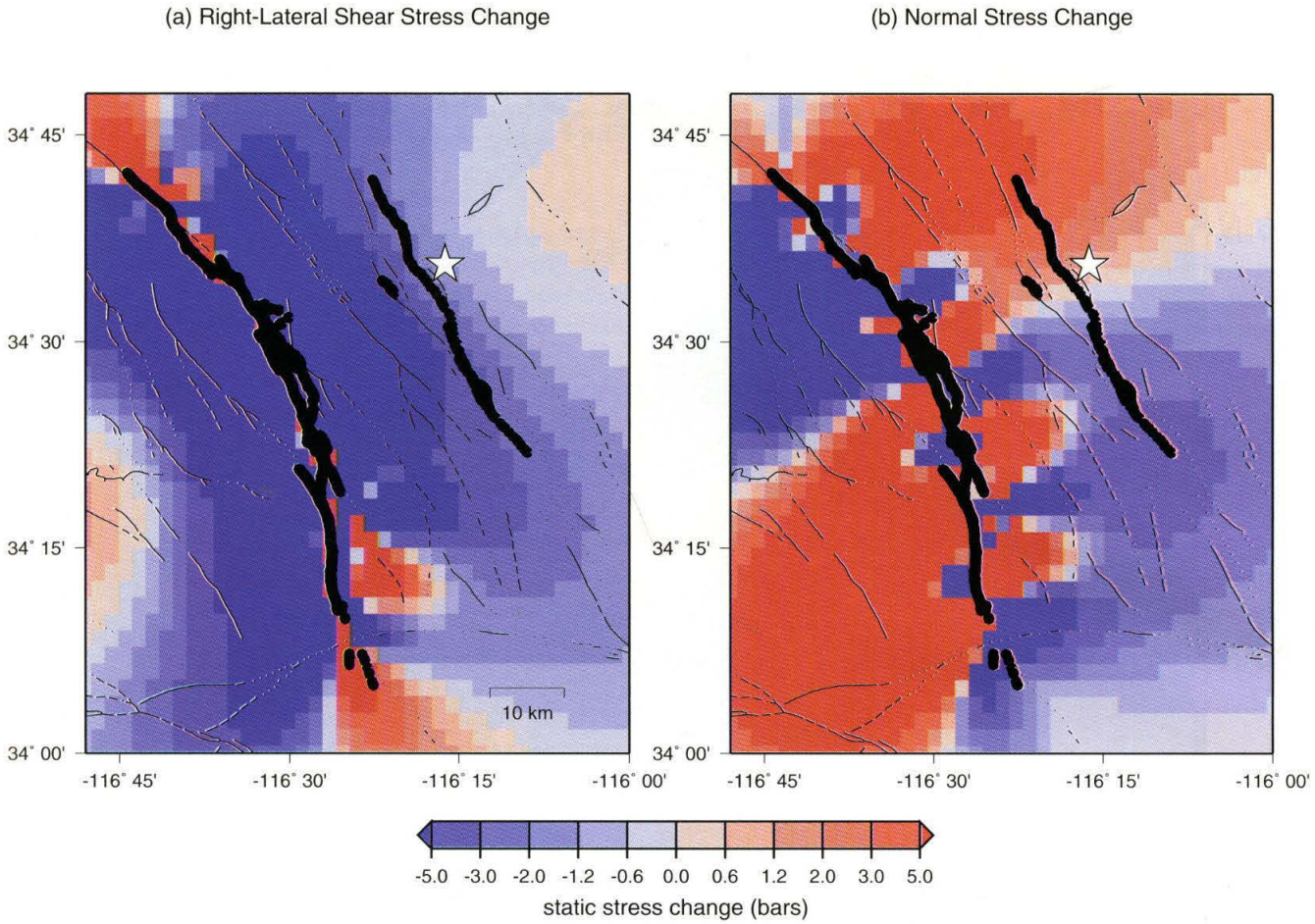

▲ **Figure 8.** Static stress changes due to the 1992 *M* 7.3 Landers earthquake, on vertical planes oriented N30°W, at 5 km depth. The Landers earthquake was modeled using the slip distribution of Wald and Heaton (1994) and static stress changes computed using the program *Elfpoint* by Robert Simpson. Surface rupture of the Landers and Hector Mine earthquakes are shown as black lines, the Hector Mine epicenter as a star. Red represents stress changes favorable to triggering; blue, unfavorable. (a) Shear stress changes, right-lateral positive. (b) Normal stress changes, tension positive.

stress change. Rupture on faults experiencing negative Coulomb stress changes due to a major earthquake is expected to be delayed. Such faults are said to be in the "stress shadow" of the earthquake (Harris and Simpson, 1996).

The Hector Mine earthquake appears to have occurred in the stress shadow of the Landers event (Figure 8). The Landers-induced shear stress change at the Hector Mine hypocenter, on a vertical plane trending N30°W, is 1.4 bar in a left-lateral sense, and the normal stress change is 1.0 bar of unclamping. This corresponds to $\Delta(CS) = -1.4$ to -0.6 bar, for m' values ranging from 0.0–0.8. The Hector Mine earthquake is therefore clearly inconsistent with triggering due to a Coulomb stress change. If normal stress changes are more important for triggering than implied by the Coulomb model, the Hector Mine event may have been triggered by the 1 bar unclamping of the fault. However, to the south of the hypocenter, where most of the rupture occurred, the normal stress change is predominantly compressional.

The uncertain relationship between the Landers and Hector Mine earthquakes presents a new challenge for earthquake-triggering research. A pair of subparallel strike-slip earthquakes appears to be at odds with the current static stress transfer view of earthquake interaction, as the first earthquake should relieve shear stress on the fault plane of the second. Static stress changes alone appear inadequate for anticipating where major earthquakes may occur, and other possible triggering mechanisms, such as changes in pore fluid pressure, will need to be explored further.

REGIONAL DISPLACEMENT FIELD FROM SCIGN

The Southern California Integrated GPS Network (SCIGN, http://www.scign.org/) is a cooperative project of the U.S. Geological Survey (USGS), Jet Propulsion Laboratory (JPL), and Scripps Institution of Oceanography (SIO). There are now approximately 140 SCIGN stations operating in southern California; an additional 110 are planned. Fortunately, several recently installed GPS stations were near the Hector Mine epicenter.

Within SCIGN, USGS is in charge of earthquake response. As part of that responsibility, USGS produced the coseismic displacements presented in Figure 9. This solution

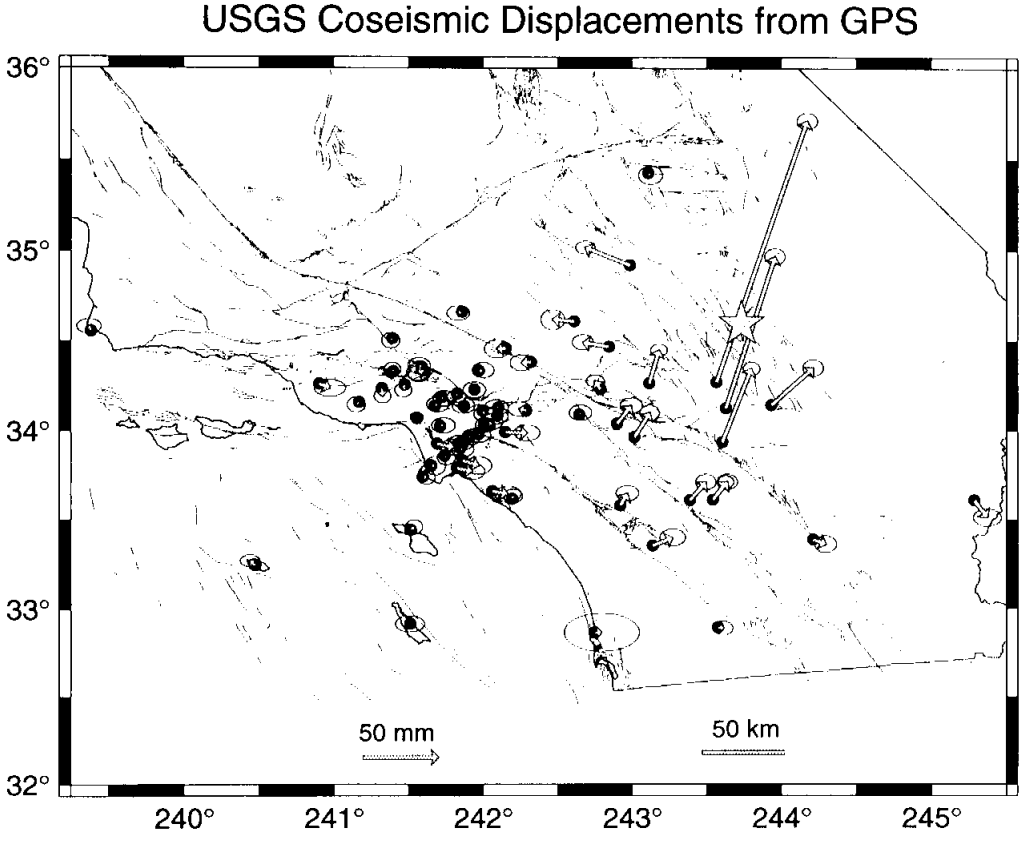

▲ **Figure 9.** USGS estimates of coseismic displacement from GPS. Error ellipses show 95% confidence area. GPS data are from the Southern California Integrated GPS Network (SCIGN).

is preliminary for two reasons. First, the solution does not include data from recently installed SCIGN stations without telemetry or from campaign-mode GPS stations now being resurveyed by several institutions with coordination by the Southern California Earthquake Center (SCEC). Second, in order to produce a solution as quickly as possible, USGS processed the data using predicted satellite orbital parameters from the International GPS Service (IGS, Beutler and Neilan, 1997). This preliminary solution will ultimately be superseded by solutions that include more stations and the contributions of the SCIGN precise processing centers (SIO, JPL).

USGS used the GAMIT software (King and Bock, 1999) to process data from 67 SCIGN stations (see Table 1). To make analysis of data from so many stations practical, stations were grouped into several subregions. Four stations from the IGS global network were included in each subregion. The positions of these reference stations were tightly constrained to their 1996 International Terrestrial Reference Frame (ITRF96, Sillard *et al.*, 1998) coordinates. The station positions, variance-covariance matrices, and other parameters from the GAMIT solution were then combined in GLOBK, a Kalman filtering routine described by Herring (1999), to produce estimates of station coordinates in the ITRF96 reference frame. As a final step, the entire southern California solution determined in GLOBK was reoriented to fit with a very well known set of thirty SCIGN station coordinates and velocities using GLOBK's GLORG reference frame stabilization module. This step removes regionwide, common-mode biases of the order 10–20 mm in the SCIGN horizontal station coordinates. Solutions from 24-hour data files for the days before and after the earthquake (days 288 and 290) were then differenced to obtain the USGS estimates of coseismic displacement.

Although we expect the final, refined solution to differ somewhat from the preliminary results shown in Figure 9, the preliminary solution is considered a robust estimate of the coseismic displacements across southern California. Significant coseismic displacements were observed at stations as distant as Blythe and Palomar, and of course throughout the Mojave Desert region. The largest motion occurred at Landers Elementary School—that site has permanently shifted 19 cm toward the north-northeast. The static displacements from these rather distant sites are consistent with very simple uniform-slip dislocation models. As of this writing, postseismic motions are only now beginning to creep above the few-millimeter noise level in SCIGN's daily measurements at some of the nearest stations. No anomalous motions of stations along the San Andreas or other neighboring faults have yet to be observed by SCIGN, though these data will certainly be analyzed carefully for any indications of strain field changes induced by this earthquake.

TABLE 1.
USGS Preliminary Coseismic Displacements from SCIGN GPS Data

			Coseismic Displacement, mm		
Site	**Latitude, deg N**	**Longitude, deg E**	**North**	**East**	**Vertical**
AOA1	34.1574	−118.8303	−1.5 ± 2.1	−1.8 ± 2.5	−4.6 ± 12.9
AVRY	34.4683	−117.1540	3.0 ± 2.1	−17.5 ± 2.9	−1.2 ± 13.0
AZU1	34.1260	−117.8965	0.4 ± 2.1	−1.3 ± 3.3	0.0 ± 13.4
BBRY	34.2643	−116.8842	22.4 ± 1.7	6.6 ± 2.3	−0.6 ± 9.7
BILL	33.5833	−117.0778	8.1 ± 2.1	4.8 ± 3.1	10.5 ± 13.4
BKMS	33.9623	−118.0947	0.2 ± 2.1	1.6 ± 2.5	−5.7 ± 12.4
BLYT	33.6104	−114.7149	−11.5 ± 2.4	8.8 ± 3.8	8.8 ± 11.1
BMRY	33.9627	−116.9847	16.3 ± 2.1	10.4 ± 2.7	8.6 ± 13.3
BRAN	34.1849	−118.2770	−0.7 ± 2.1	1.6 ± 3.0	3.3 ± 13.2
BSRY	34.9186	−117.0120	11.9 ± 1.8	−30.0 ± 2.7	−1.5 ± 10.4
CAT1	33.4458	−118.4830	2.0 ± 1.9	2.2 ± 2.4	−4.9 ± 11.8
CHIL	34.3334	−118.0260	0.4 ± 2.1	2.8 ± 3.0	−2.0 ± 13.3
CIT1	34.1367	−118.1273	0.3 ± 2.1	−0.3 ± 3.1	−4.2 ± 12.9
CLAR	34.1099	−117.7088	1.3 ± 2.0	−4.6 ± 3.1	−4.5 ± 12.7
CMP9	34.3532	−118.4114	1.2 ± 2.2	−1.6 ± 3.1	3.5 ± 13.9
CRFP	34.0391	−117.0997	12.1 ± 2.1	9.6 ± 3.1	4.7 ± 12.9
CSDH	33.8615	−118.2567	−1.5 ± 1.9	1.2 ± 2.5	−4.1 ± 12.2
CSN1	34.2536	−118.5238	−3.4 ± 1.9	−1.0 ± 2.3	−1.5 ± 11.7
CTMS	34.1241	−116.3704	101.9 ± 2.2	32.9 ± 2.8	17.8 ± 12.9
CVHS	34.0820	−117.9017	0.5 ± 2.3	−0.5 ± 3.2	−6.2 ± 14.2
DAM1	34.3340	−118.3974	−2.0 ± 2.2	−3.0 ± 3.0	−4.6 ± 14.1
DAM2	34.3348	−118.3969	−1.1 ± 2.3	−3.8 ± 3.1	1.1 ± 14.8
DHLG	33.3898	−115.7880	−3.1 ± 2.3	8.4 ± 3.0	7.3 ± 12.8
DYHS	33.9380	−118.1260	−0.3 ± 2.0	0.2 ± 2.5	−2.0 ± 12.4
FHFF	34.5139	−118.6083	−1.3 ± 2.1	−0.9 ± 2.5	3.3 ± 12.5
FVPK	33.6623	−117.9357	−1.9 ± 2.2	10.3 ± 3.6	5.4 ± 13.9
GOL2	35.4252	−116.8893	−1.4 ± 2.5	1.4 ± 3.3	−4.8 ± 10.1
HOLC	34.4582	−117.8452	−0.2 ± 2.5	−5.9 ± 3.5	−2.3 ± 15.0
HOLP	33.9245	−118.1682	0.3 ± 2.2	−0.1 ± 2.6	1.4 ± 13.2
JPLM	34.2048	−118.1732	−1.8 ± 1.6	−0.3 ± 2.6	5.4 ± 10.3
LASC	33.9279	−118.3065	−2.3 ± 2.2	11.1 ± 3.6	−4.9 ± 13.7
LBC1	33.8321	−118.1372	−3.1 ± 2.4	10.9 ± 3.6	4.4 ± 14.6
LBC2	33.7916	−118.1732	−2.1 ± 2.2	10.0 ± 3.6	0.7 ± 13.8
LDES	34.2673	−116.4328	175.5 ± 2.3	60.7 ± 2.8	26.8 ± 13.3
LEEP	34.1346	−118.3217	1.4 ± 2.1	1.9 ± 3.0	2.1 ± 12.9
LINJ	34.6600	−118.1400	−0.6 ± 2.1	−2.5 ± 3.1	5.3 ± 13.4
LONG	34.1119	−118.0034	−2.3 ± 2.1	1.6 ± 3.0	−7.3 ± 13.5
LPHS	34.0268	−117.9567	2.7 ± 2.1	1.3 ± 3.1	−10.2 ± 13.8
MONP	32.8919	−116.4224	−0.3 ± 1.9	3.5 ± 2.6	−0.7 ± 9.7
MSOB	34.2308	−117.2101	5.5 ± 1.7	−3.5 ± 2.5	−0.5 ± 10.3

TABLE 1. (Continued)
USGS Preliminary Coseismic Displacements from SCIGN GPS Data

			Coseismic Displacement, mm		
Site	**Latitude, deg N**	**Longitude, deg E**	**North**	**East**	**Vertical**
MUSD	34.2616	−119.0961	−2.9 ± 2.3	7.1 ± 4.3	−2.1 ± 14.0
OAES	34.1410	−116.0677	25.2 ± 2.3	28.1 ± 2.8	0.9 ± 13.1
OAT2	34.3299	−118.6014	1.3 ± 1.9	−0.5 ± 2.3	4.9 ± 12.0
PIN1	33.6122	−116.4582	12.2 ± 1.7	8.8 ± 2.2	3.7 ± 9.4
PIN2	33.6122	−116.4576	12.3 ± 2.1	9.8 ± 2.8	3.1 ± 12.5
PMHS	33.9026	−118.1537	−0.8 ± 2.1	1.7 ± 3.1	−4.4 ± 13.3
PMOB	33.3572	−116.8595	5.4 ± 2.3	13.3 ± 3.5	0.6 ± 14.2
PVEP	33.7433	−118.4042	−0.3 ± 1.9	2.7 ± 2.4	−1.4 ± 11.9
ROCH	33.6110	−116.6098	12.3 ± 2.1	10.6 ± 2.8	5.1 ± 12.8
ROCK	34.2357	−118.6764	−5.2 ± 1.9	0.4 ± 2.3	8.4 ± 12.0
RTHS	34.0892	−117.3533	1.3 ± 2.1	0.9 ± 3.1	−0.5 ± 13.1
SCIA	34.6075	−117.3883	1.4 ± 2.8	−14.2 ± 3.3	0.6 ± 15.7
SCIP	32.9144	−118.4881	0.1 ± 2.2	−0.1 ± 4.0	−4.0 ± 11.7
SIO3	32.8647	−117.2504	0.2 ± 5.2	4.8 ± 10.3	−6.8 ± 24.2
SNI1	33.2479	−119.5244	3.0 ± 1.6	−3.4 ± 2.7	5.2 ± 8.5
SPMS	33.9927	−117.8488	−0.5 ± 2.2	14.6 ± 3.5	−2.5 ± 13.7
SPMX	31.0500	−115.4700	−7.4 ± 2.7	−1.1 ± 4.9	−5.0 ± 14.6
TABL	34.3819	−117.6783	−0.4 ± 2.2	−6.4 ± 3.1	−3.2 ± 13.6
TORP	33.8040	−118.3452	0.1 ± 2.5	2.6 ± 2.8	−12.5 ± 15.8
TRAK	33.6179	−117.8034	2.1 ± 1.9	0.6 ± 2.6	2.0 ± 12.1
UCLP	34.0691	−118.4419	0.7 ± 1.3	−0.2 ± 1.8	5.9 ± 8.4
USC1	34.0239	−118.2851	0.7 ± 2.1	2.1 ± 3.2	4.3 ± 13.7
VNDP	34.5563	−120.6165	3.1 ± 2.0	−1.3 ± 3.3	2.3 ± 10.0
VYAS	34.0309	−117.9921	0.2 ± 2.0	0.5 ± 2.5	−4.6 ± 12.6
WHC1	33.9799	−118.0312	−0.3 ± 2.0	0.8 ± 3.1	−3.9 ± 12.7
WIDC	33.9348	−116.3918	49.4 ± 1.8	19.4 ± 2.3	10.9 ± 9.8
WLSN	34.2261	−118.0559	0.0 ± 2.2	−0.1 ± 3.1	−1.8 ± 14.0

THE HECTOR MINE SEQUENCE: AFTERSHOCKS AND TRIGGERED SEISMICITY

The results presented so far have focused specifically on investigations of the Hector Mine mainshock. Yet abundant data has also been collected from the entire Hector Mine sequence, which includes an aftershock sequence that appears to be about average for a M 7.1 event. Within the first two weeks of the mainshock, over 2,500 aftershocks were recorded, including a half-dozen of M 5.0 or larger. The largest aftershock was a M 5.8 event at 5:57 A.M. local time (12:57 GMT) on 10/16.

Using data from both the high gain analog stations of the Southern California Seismic Network (SCSN) and the new TriNet stations, we have relocated the foreshocks, mainshock, and aftershocks using the three-dimensional velocity model of Hauksson (1999). The preliminary results illustrate the spatial relationships between the causative faults and the hypocenters of the foreshocks, mainshock, and aftershocks (Figure 1).

The aftershocks delineate the entire rupture zone. Several pockets of high aftershock activity have persisted, including several near bends in the fault rupture, near the northernmost end of the rupture, and one approximately 10 km north of that. The seismotectonics of this region, which appears to correspond to a complex zone of fault bending and fault interactions, will be explored in future analyses using high-resolution hypocentral relocation techniques and focal mechanism analysis.

In addition to the classic aftershock sequence, the Hector Mine earthquake was noteworthy in that it appeared to "light up" seismicity over much of southern California, par-

ticularly southwest of the epicenter. The phenomenon of "triggered events" was first documented convincingly following the 1992 Landers earthquake (Bodin and Gomberg, 1994; Hill *et al.*, 1993). Whereas the Landers earthquake triggered regional seismicity to the north, preliminary results indicate that events triggered by the Hector Mine earthquake were predominantly to the south. This contrast may reflect the different directivities of the two mainshocks.

Among the apparently triggered events to the south were a relatively small number that occurred near the southern end of the Salton Sea, close to the southern terminus of the San Andreas Fault. In the early aftermath of the mainshock, these events raised a measure of concern for the possible effect of the mainshock on the San Andreas system. At the time of this writing (two and a half weeks after the mainshock), the triggered events appear to have died down. Subsequent detailed analyses will focus on the distribution and characteristics of the triggered events in the context of the static and dynamic stress changes produced by the mainshock.

DISCUSSION AND CONCLUSIONS

At first glance the 1992 Landers and 1999 Hector Mine earthquakes appear to be similar. In addition to the similar orientations, styles of faulting, and seismotectonic setting, both events caused triggered seismicity beyond their immediate aftershock zones.

Yet within days of the Hector Mine mainshock, it became apparent that a number of interesting and important scientific issues have been raised by this event. These issues include the nature of rupture processes in zones of distributed, low slip-rate faulting, the effect of static (Coulomb) stress change, the physical mechanisms associated with triggered seismicity, and the effect of the Hector Mine earthquake on the southern San Andreas Fault.

The Hector Mine earthquake generated a diverse, abundant geological and geophysical data set, largely by virtue of having been the first significant earthquake in southern California to occur when both the SCIGN and TriNet projects were well underway. The effective integration of these projects with the World Wide Web allowed for rapid dissemination of data and results. This rapid response was appreciated by both the local media and residents of southern California, who dubbed Hector Mine the first-ever "cyberquake." It also made available abundant high-quality data with which the interesting scientific questions can be addressed quickly. Although definitive results will require more detailed analyses, the preliminary results presented in this paper illustrate the kinds of investigations that are now possible within just two weeks of a significant earthquake, if the right kinds of data and tools are available.

ACKNOWLEDGMENTS

We acknowledge Andy Michael and Nano Seeber for helpful and timely reviews of this manuscript. We thank Lt. Col. James J. Tabak, Captain Teitzel, Mr. Paul "Kip" Otis-Deihl, the Explosive Ordinance Disposal Section, the Range Operations Section, Range Control, and the command and personnel of Marine Corp Air Ground Combat Center, Twenty-Nine Palms, California, for their tremendous assistance and cooperation in facilitating field investigations. We also thank CWO4 T. Murphy, 1st Lt. J. Ochwatt, and SPC4 B. V. Cabanban, Jr. of the Los Alamitos Army Aviation Support Facility, California Army National Guard. The TriNet project is funded by FEMA/OES, USGS, and Caltech private-sector partners. We acknowledge the Southern California Integrated GPS Network (sponsored by the W. M. Keck Foundation, NASA, NSF, USGS, SCEC) for providing data used in this study. SCEC is funded by NSF Cooperative Agreement EAR-8920136, USGS Cooperative Agreement 1434-HQ-97AG01718, and California Department of Transportation Contract 59A0050. Caltech Seismology Laboratory contribution #8685. SCEC contribution #494.

CONTRIBUTORS

Jeff Behr, Bill Bryant, Doug Given, Karl Gross, Katrin Hafner, Jeanne Hardebeck, Egill Hauksson, Tom Heaton, Susan Hough, Ken Hudnut, Kate Hutton, Lucy Jones, Hiroo Kanamori, Katherine Kendrick, Nancy King, Phil Maechling, Aron Meltzner, Dan Ponti, Tom Rockwell, Anthony Shakal, Mark Simons, K. Stark, David Wald, Lisa Wald, and Lupei Zhu.

Contacts for Further Information

S. Hough, U.S. Geological Survey, Pasadena, CA 91106; hough@gps.caltech.edu

E. Hauksson, Caltech, Pasadena, CA 91025; hauksson@gps.caltech.edu

W. Bryant, California Division of Mines and Geology, Sacramento, CA; bbryant@consrv.ca.gov

REFERENCES

Beutler, G. and R. Neilan (1997). International GPS Service for Geodynamics, International Association of Geodesy General Assembly, Rio de Janeiro, Brazil, September 3–9, 1997.

Bodin, P. and J.S. Gomberg (1994). Triggered seismicity and deformation between the Landers, California, and Little-Skull-Mountain, Nevada, earthquakes, *Bull. Seism. Soc. Am.* **84**, 835–843.

Dengler, L.A. and J.W. Dewey (1998). An intensity survey of households affected by the Northridge, California, earthquake of 17 January, 1994, *Bull. Seism. Soc. Am.* **88**, 441–462.

Dibblee, T.W., Jr. (1966). Geologic map of the Lavic quadrangle, San Bernardino County, California, *U.S. Geological Survey Miscellaneous Geologic Investigations Map I-472*, map scale 1:62,500.

Dibblee, T.W., Jr. (1967a). Geologic map of the Deadman Lake quadrangle, San Bernardino County, California, *U.S. Geological Survey Miscellaneous Geologic Investigations Map I-488*, map scale 1:62,500.

Dibblee, T.W., Jr. (1967b). Geologic map of the Emerson Lake quadrangle, San Bernardino County, California, *U.S. Geological Survey*

Miscellaneous Geologic Investigations Map I-490, map scale 1:62,500.

Dokka, R.K. and C.J. Travis (1990). Late Cenozoic strike-slip faulting in the Mojave Desert, California, *Tectonics* **9**, 311–340.

Hadley, D. and H. Kanamori (1979). Regional *S*-wave structure for southern California from the analysis of teleseismic Rayleigh waves, *Geophys. J. R. Astr. Soc.* **58**, 655–666.

Harris, R.A. and R.W. Simpson (1996). In the shadow of 1857: The effect of the great Ft. Tejon earthquake on subsequent earthquakes in southern California, *Geophys. Res. Lett.* **23**, 229–232.

Hart, E.W. (1987). *Pisgah, Bullion, and Related Faults, San Bernardino County, California*, California Division of Mines and Geology Fault Evaluation Report FER-188, 19 pp. (unpublished).

Hart, E.W. and W.A. Bryant (1997). *Fault-rupture Hazard Zones in California*, Department of Conservation, Division of Mines and Geology Special Publication, 42, 38 pp.

Hauksson, E., L.M. Jones, K. Hutton, and D. Eberhart-Phillips (1993). The 1992 Landers earthquake sequence: Seismological observations, *J. Geophys. Res.* **98**, 19,835–19,858.

Hauksson, E. (1999). Crustal structure and seismicity distribution adjacent to the Pacific and North America Plate boundary in southern California, *J. Geophys. Res.*, in press.

Hauksson, E., L.M. Jones, and A. Shakal (1999). TriNet, *International Handbook of Earthquake and Engineering Seismology: Centennial Publication of the International Association of Seismology and Physics of the Earth's Interior*, Paul Jennings, Hiroo Kanamori, and Willie Lee, editors, submitted.

Herring, T. (1999). *Documentation of the GLOBK Software version 5.1*, Massachusetts Institute of Technology, Cambridge, Massachusetts.

Hill, D.P., P.A. Reasenberg, A. Michael, W.J. Arabasz, G. Beroza, D. Brumbaugh, J.N. Brune, R. Castro, S. Davis, D. dePolo, W.L. Ellsworth, J. Gomberg, S. Harmsen, L. House, S.M. Jackson, M.J.S. Johnston, L. Jones, R. Keller, S. Malone, L. Munguia, S. Nava, J.C. Pechmann, A. Sanford, R.W. Simpson, R.B. Smith, M. Stark, M. Stickney, A. Vidal, S. Walter, V. Wong, J. Zollweg (1993). Seismicity remotely triggered by the magnitude 7.3 Landers, California, earthquake, *Science* **260**, 1,617–1,623.

Kanamori, H., J. Mori, E. Hauksson, T.H. Heaton, L.K. Hutton, and L.M. Jones (1993). Determination of earthquake energy-release and M(L) using TERRAscope, *Bull. Seism. Soc. Am.* **83**, 330–346.

King, R.W. and Y. Bock (1999). *Documentation of the GAMIT GPS Analysis Software version 9.8*, Massachusetts Institute of Technology, Cambridge, Massachusetts.

Mori, J., H. Kanamori, J. Davis, E. Hauksson, R. Clayton, T. Heaton, L. Jones, and A. Shakal (1999). Major improvements in progress for southern California earthquake monitoring, *Trans. Am. Geophys. U.* **79**, 217–221.

Sauber, J., W. Thatcher, and S.C. Solomon (1986). Geodetic measurement of deformation in the central Mojave Desert, California, *J. Geophys. Res.*, **91**, 2,683–2,693.

Sauber, J., W. Thatcher, S.C. Solomon, and M. Lisowski (1994). Geodetic slip rate for the eastern California shear zone and the recurrence time of Mojave Desert earthquakes, *Nature* **367**, 264–266.

Sieh, K., L. Jones, E. Hauksson, K. Hudnut, D. Eberhart-Phillips, T. Heaton, S. Hough, K. Hutton, H. Kanamori, A. Lilje, S. Lindvall, S.F. McGill, J. Mori, C. Rubin, J.A. Spotila, J. Stock, H.K. Thio, J. Treiman, B. Wernicke, and J. Zachariasen (1993). Near-field investigations of the Landers earthquake sequence, April to July 1992, *Science* **260**, 171–176.

Sillard, P., Z. Altamimi, and C. Boucher (1998). The ITRF96 realization and its associated velocity field, *Geophys. Res. Lett.* **17**, 3,223–3,226.

Wald, L.A., L.K. Hutton, and D.D. Given (1995). The Southern California Network Bulletin: 1990–1993 summary, *Seism. Res. Lett.* **66**, 9–19.

Wald, D.J., V. Quitoriano, T. Heaton, and H. Kanamori (1999a). Relationships between peak ground acceleration, peak ground velocity, and Modified Mercalli Intensity in California, *Earthquake Spectra* **15**, 557–564.

Wald, D.J., V. Quitoriano, T. Heaton, H. Kanamori, C.W. Scrivner, and C.B. Worden (1999b). TriNet "ShakeMaps": Rapid generation of instrumental ground motion and intensity maps for earthquakes in southern California, *Earthquake Spectra* **15**, 537–556.

Wald, D.J., V. Quitoriano, L. Dengler, and J.W. Dewey (1999c). Utilization of the Internet for rapid community seismic intensity maps, *Seism. Res. Lett.*, **70**, 680–697.

Wesnousky, S. (1986). Earthquakes, Quaternary faults, and seismic hazard in California, *J. Geophys. Res.* **91**, 2,587–2,631.

Zhu, L. and D.V. Helmberger (1996). Advancement in source estimation techniques using broadband regional seismograms, *Bull. Seism. Soc. Am.* **86**, 1,634–1,641.